Published in final edited form as:
Neuroimage. 2008 November 15; 43(3): 447–457. doi:10.1016/j.neuroimage.2008.07.009.

Human Brain White Matter Atlas: Identification and Assignment of Common Anatomical Structures in Superficial White Matter

Kenichi Oishi[1], **Karl Zilles**[6,7], **Katrin Amunts**[6,8], **Andreia Faria**[1], **Hangyi Jiang**[1,2], **Xin Li**[2], **Kazi Akhter**[1], **Kegang Hua**[1,2], **Roger Woods**[4], **Arthur W. Toga**[4], **G. Bruce Pike**[5], **Pedro Rosa-Neto**[5], **Alan Evans**[5], **Jiangyang Zhang**[1], **Hao Huang**[1], **Michael I. Miller**[3], **Peter C.M. van Zijl**[1,2], **John Mazziotta**[4], and **Susumu Mori**[1,2]

1*The Russell H. Morgan Department of Radiology and Radiological Science, The Johns Hopkins University School of Medicine, Baltimore, MD, USA*

2*F.M. Kirby Research Center for Functional Brain Imaging, Kennedy Krieger Institute, Baltimore, MD, USA*

3*Department of Biomedical Engineering, The Johns Hopkins University School of Medicine, Baltimore, MD, USA*

4*Department of Neurology, University of California Los Angels, School of Medicine, Los Angels, CA, USA*

5*McConnell Brain Imaging Centre, Montreal Neurological Institute, McGill University, Montreal, Canada*

6*Institute of Neuroscience and Biophysics INB-3, Research Centre Jülich, Jülich, Germany*

7*C. & O. Vogt Institute of Brain Research, Heinrich-Heine-University of Düsseldorf, Düsseldorf, Germany*

8*Department of Psychiatry and Psychotherapy, RWTH Aachen University, Aachen, Germany*

Abstract

Structural delineation and assignment are the fundamental steps in understanding the anatomy of the human brain. The white matter has been structurally defined in the past only at its core regions (deep white matter). However, the most peripheral white matter areas, which are interleaved between the cortex and the deep white matter, have lacked clear anatomical definitions and parcellations. We used axonal fiber alignment information from diffusion tensor imaging (DTI) to delineate the peripheral white matter, and investigated its relationship with the cortex and the deep white matter. Using DTI data from 81 healthy subjects, we identified nine common, blade-like anatomical regions, which were further parcellated into 21 subregions based on the cortical anatomy. Four short association fiber tracts connecting adjacent gyri (U-fibers) were also identified reproducibly among the healthy population. We anticipate that this atlas will be useful resource for atlas-based white matter anatomical studies.

Keywords

human; white matter; atlas; association fiber; magnetic resonance imaging; diffusion tensor

Corresponding author: Susumu Mori, PhD The Russell H. Morgan Department of Radiology and Radiological Science The Johns Hopkins University School of Medicine 217 Traylor Building 720 Rutland Avenue Baltimore, MD 21205 Work: 410−614−2702 Email: Susumu@mri.jhu.edu.

Introduction

Although the anatomy of the human brain has been studied extensively for over a century, there still remain many anatomical features that are difficult to characterize. One of the greatest challenges is the understanding of the cortical structures, which are known to be extensively heterogeneous, both regionally and across subjects (Zilles, 2004). White[S1] matter (WM) structures seem to share more common anatomical features across individuals at the deep white matter regions (DWM); there are many prominent axonal bundles that can be identified in all normal subjects at well-defined locations (Dejerine, 1895; Flechsig, 1920)[S2](Axer and Keyserlingk, 2000; Burgel et al., 1997; Burgel et al., 1999; Clarke and Miklossy, 1990). However, the peripheral, more superficially located white matter (SWM), which fills the space between the DWM and the cortex, has not been well characterized in the past. For example, the SWM is known to contain short cortical association fibers, but their location, number, and trajectories are not sufficiently defined.

This lack of anatomic knowledge about the SWM is understandable. The 3D axonal anatomy is, in general, difficult to understand by inspection of 2D histological sections. The entire WM of the adult human brain looks more or less homogeneous, both in myelin stained histological sections and in macroscopical slabs of native or fixed brains. The anatomy of very large fiber bundles can be studied by freezing and thawing repeatedly postmortem brains and subsequent manual peeling of fiber bundles (Krieg, 1963). This approach, however, cannot isolate smaller fibre bundles. Finally, population studies of the intersubject variability of SWM fiber tracts are still lacking.

In the past, atlases of the gray matter based on histology and MRI have been introduced, including probabilistic maps (Amunts and Zilles, 2001; Eickhoff et al., 2005; Toga et al., 2006). However, WM atlases are scarce (Burgel et al., 2006), and do not provide population-based SWM mapping.

Diffusion tensor imaging (DTI) is an MRI modality that can delineate WM structures based on the orientation information of axons (Basser et al., 1994; Makris et al., 1997; Mori et al., 2005; Pierpaoli et al., 1996; Wakana et al., 2004). This is[S3] a well-suited method for investigating the anatomy of the WM and for performing group-based analyses.

In our previous studies, we generated a DTI database of a normal population under an initiative of the International Consortium of Brain Mapping (ICBM) and created a population-averaged map of WM anatomy using data from 81 subjects (ICBM-DTI-81 atlas, http://www.loni.ucla.edu/Atlases,lbam.med.jhmi.edu). Using this map, we generated a hand-segmented atlas of 50 DWM structures (Mori et al., 2008a) that have been well-documented in the classical histological studies. The[S4] aim of this study was to investigate whether we can extend this atlas to the SWM regions by identifying structures common to normal brains. We used the population-averaged tensor map to identify features in the SWM that were common across normal subjects. These common structures were segmented in the ICBM-152 (Mazziotta et al., 1995) coordinates. The present paper describes the anatomy of the SWM. We believe that this atlas will be a useful resource to anatomically identify WM regions affected by diseases or peripheral white matter lesions, or to use as a template for automated WM parcellation.

Methods

Data acquisition and creation of the population-averaged atlas in the ICBM-152 coordinates (ICBMDTI-81)

DTI data obtained from 81 normal subjects were used for the population-averaged atlas. The data were acquired at the Montreal Neurological Institute (24 subjects) and University of California Los Angeles (57 subjects) under the International Consortium of Brain Mapping (ICBM) collaboration (M: 42, F: 39, average age: 38. 63 (18 − 59 years old), right-handed) as described before (Mori et al., 2008a). The data were obtained on Siemens 1.5T MR units. DTI[S5] data were acquired using single-shot echo-planar imaging sequences with sensitivity encoding (SENSE) and a parallel imaging factor of 2.0 (Pruessmann et al., 1999). The imaging matrix was 96 × 96, with a field of view of 240 × 240 mm (nominal resolution: 2.5mm). Transverse sections of 2.5 mm thickness were acquired parallel to the anterior commissure-posterior commissure line (AC-PC). A total of 60 sections covered the entire hemisphere and brainstem without gaps. Diffusion weighting was encoded along 30 independent orientations (Jones et al., 1999), and the b-value was 1,000 s/mm^2. Five additional images with minimal diffusion weighting (b = 33mm^2/sec) were also acquired. The scanning time per dataset was approximately four minutes. To enhance the signal-to-noise ratio, imaging was repeated twice.

The raw diffusion-weighted images (DWIs) were first co-registered to one of the least diffusion-weighted images and corrected for Eddy current and subject motion with affine transformation using Automated Image Registgration (AIR) (Woods et al., 1998). The average of all DWIs (aDWI) was calculated and used for DTI-based anatomic image. The six elements of the diffusion tensor were calculated for each pixel with multivariate linear fitting using DtiStudio (H. Jiang and S. Mori, Johns Hopkins University, Kennedy Krieger Institute) (Basser et al., 1994; Jiang et al., 2006). After diagonalization, three eigenvalues and eigenvectors were obtained. For the anisotropy map, fractional anisotropy (FA) was used (Pierpaoli and Basser, 1996). The eigenvector (v1) associated with the largest eigenvalue was used as an indicator for fiber orientation. A 24-bit color-coded orientation map was created by assigning red, green, and blue channels to the x (right-left), y (anterior-posterior), and z (superior-inferior) components of the v1 and its intensity was modulated by FA.

For anatomical images to drive the normalization process, aDWIs were used. These images were normalized to the template (ICBM-152) using a 12-channel affine non-linear transformation of AIR. The transformation matrix was then applied to the calculated diffusion tensor field, based on the method described by Alexander and Gee (Alexander et al., 2001) and Xu et al. (Xu et al., 2003). The entire normalization process was performed by in-house software called Landmarker (X. Li, H. Jiang, and S. Mori, Johns Hopkins University, lbam.med.jhmi.edu or www.DtiStudio.org) and took approximately 30 min [S6] . After normalization, the image matrix and pixel resolution were interpolated to match those of the ICBM-152 (181 × 217 × 181 with 1 mm pixel resolution) using trilinear interpolation. To obtain population-averaged data, the linearly transformed tensor fields from individual subjects were averaged by simple scalar averaging of tensor elements. From the averaged tensor field, the FA and color-coded maps were recalculated.

Parcellation of the gray matter

We used maximum likelihood maps, which identify the most likely gyrus at each voxel in the atlas space, provided by the Laboratory of Neuro Imaging (LONI), University of California, Los Angeles. This is called The LONI Probabilistic Brain Atlas (LPBA40) and can be downloaded from the website (http://www.loni.ucla.edu/Atlases/). The[S7] atlas contains 24 gyri labels.

Parcellation of the WM

We[S8] first defined the WM / cortex boundary using an FA threshold of 0.25 in each subject. Since our aim was to delineate the common SWM structure across the subjects for DTI analysis, we set this threshold to minimize the inclusion of the cortex, which typically has FA less than 0.15. Please note that this boundary does not represent the cortex – WM boundary typically defined by T1-weighted images. The defined white matter was converted to binary images (inside the boundary = 1; outside the boundary = 0) and transformed to the template. The binary maps obtained from the 81 subjects were normalized to the template and averaged to obtain a *"probabilistic"* WM map in each pixel in the ICBM152 coordinates. For the parcellation of the DWM, we used our previous WM parcellation map (WMPM) (Mori et al., 2008a)[S9]. The SWM was defined as the WM between the WMPM and the cortex using thresholds applied to the probabilistic WM map.

Tractography for short association fibers

For tractography, the Fiber Assignment by Continuous Tracking (FACT) method (Mori et al., 1999; Xue et al., 1999) was used. The fiber tracking was performed[S10] in DtiStudio. The two-ROI approach was applied to reconstruct tracts of interest (Conturo et al., 1999; Huang et al., 2004). The[S11] two ROIs were defined by parcellated SWM regions as will be described in the Result section. We first performed the tractography using the ICBM-DTI-81 with a fractional anisotropy threshold of 0.15 and fiber angles of less than 40^{o} between two connected pixels. The results were confirmed using individual data from 10 normal subjects, in which the anisotropy threshold was increased to 0.25. We used lower FA threshold for the population-averaged ICBM-DTI-81 data because the linear tensor averaging adopted in this study leads to lower FA due to orientation variability of the tensors among individuals.

Results

Identification of common structures in the SWM

Fig. 1A and B show axial slices of ICBM-152 (population-averaged T1-weighted image) and ICBM-DTI-81 (population-averaged color-coded map). The DTI-based image clearly visualizes various intra-WM structures that cannot be appreciated by the conventional T1-weighted image. Anatomy of the DWM areas, which consist of large axonal bundles, has been well-characterized in the past by the anatomical or histological studies of (Dejerine, 1895) and (Flechsig, 1920). Figs. 1B - D show the hand-parcellated map of the DWM based on such existing knowledge (WMPM) (Mori et al., 2008a). These anatomical structures can be clearly identified in the population-averaged maps (Fig. 1B), indicating that their existence and locations are common among normal subjects. By superimposing the WMPM to the probabilistic WM map (Fig. 1C), the white matter probability of the 50 structures in the WMPM was found to be high (0.86 ± 0.10). The exception was the fornix, which had only 0.43 because of its small size and non-perfect registration by the affine transformation. From the probabilistic WM map (Fig. 1C), it is also clear that there are many regions in the SWM with high probability. In Fig. 1E and F, the SWM is three-dimensionally (3D) visualized using a WM probability threshold of 0.6, with (Fig.1E) and without (Fig.1F) the DWM parcellation. This image represents the SWM structures that are common in the normal population, but have not been well characterized in the past (CSWM, hereafter). Fig. 2 shows the anatomy of the CSWM, visualized by different threshold levels.

Assignment of common structures in the SWM

As can be seen in Figs. 2, the CSWM was morphologically constructed by several "blade-like" structures (called "blade," hereafter), that often seem to extend across multiple gyri. Based on the structures of these blades, we manually divided them into nine distinctive blades (Fig.2).

We named each blade as follows: superior frontal blade (SF); middle frontal blade (MF); inferior frontal blade (IF); pre-central blade (PrC); post-central blade (PoC); superior parietal blade (SP); parieto-temporal blade (PT); temporal blade (Tmp); and occipital blade (Oc). The blades can be identified even after the probability threshold is increased to 0.9, except for the MF which can be identified with the threshold of 0.8 (Figs 2A-3D). To demonstrate that these blades are reproducible structures common to normal subjects, we parcellated the CSWM into the nine blades in data from 10 subjects who were not used for ICBM-DTI-81; five of these are shown in Fig. 3. While there is noticeable inter-subject variability in terms of the shapes of the blades, these nine blades were consistently identified in all subjects.

In Fig. 4D-4F, three-dimensional views of the maximum likelihood atlas of the gray matter in the ICBM coordinates (LPBA40.AIR) are shown and compared to the CSWM thresholded by probability 0.6 (Fig. 4A-4C). Because the borders of the blades usually coincide with the borders of cortical parcellation, there is a relatively simple relationship between the two; namely, there is a one-to-one correspondence or there are multiple subparcellations within one blade. We can also say that from the blade-type CSWM anatomical features, only nine borders can be defined out of the 27 gyri-based parcellations. The only exception is the fusiform WM, which spans the temporal blade and the occipital blade.

Based on this cortical parcellation information, the CSWM with the probability over 0.6 were parcellated, as shown in Table 1. Here, we subparcellated the CSWM based on their relationships with the 24 gyri. The sub-parcellated regions are named “gyrus name”-WM as follows: superior frontal WM; middle frontal WM; inferior frontal WM; pre-central WM; rectus WM; middle orbito-frontal WM; lateral orbito-frontal WM; post-central WM; superior parietal WM; supramarginal WM; angular WM; precuneus WM; superior occipital WM; middle occipital WM; inferior occipital WM; cuneus WM; lingual WM; superior temporal WM; middle temporal WM; inferior temporal WM; and fusiform WM. Note that WM regions that correspond to the cingulate gyrus, the insula, and the parahippocampal gyrus were difficult to identify because they face major WM tracts (the cingulum, the external capsule, and the stria terminalis / cingulum) directly, and therefore, there is no CSWM associated with them.

Fiber structures of the CSWM and inter-blade connections

Inside these blades, fibers primarily run along the radial orientation of the blades (Fig. 5A). Therefore, we did not find reproducible patterns of intra-blade fibers that can be clearly identified by tractography. Once[S12] the traced tracts exit the blade, majority of these tracts merges with one of the major white matter bundles in the DWM. We performed tractography by using the 9 blades as ROIs for trajectory selections. As expected, inter-blade tractography identifies most major long association fibers, which have been extensively documented by histology and tractography in the past. The results are provided in Table 2. Among these long association fibers, the superior longitudinal fascicle is defined as a collection of four different inter-blade connections, which agrees with previous reports and is denoted as the SLF-I, II, III, and arcuate fibers (Ar) (Catani et al., 2005;Makris et al., 2005;Petrides and Pandya, 1984).

Among these inter-blade fibers, those not previously delineated in detail are shown in Figs. 5B and 5C. These were designated as follows: frontal short association fibers (connecting the superior frontal blade and the inferior frontal blade); fronto-central short association fibers (connecting the middle frontal blade and the pre-central blade); central short association fibers (connecting the pre- and post- central blades); parietal short association fibers (connecting the superior parietal blade and the parieto-temporal blade); and parieto-temporal long association fibers (connecting the superior parietal blade and the parieto-temporal blade / temporal blade). Their locations in the ICBM-152 coordinates are shown in Fig. 6.

To demonstrate that these inter-blade association fibers are common to normal subjects, we performed tract tracing in data from 10 subjects who were not included in ICBM-DTI-81, and five of these are shown in Fig. 7. The fronto-central, central, and parietal short association fibers can be readily appreciated in all subjects. However, the frontal short association fibers were not reproducible in three of 10 subjects; in these three subjects, the fibers were fragmented into two sections (superior-middle frontal blade connections and middle-inferior blade connections). We could not find parieto-temporal long association fibers in two of 10 subjects, and four of 10 subjects had the fibers only on one side (two subjects on the right side only and two subjects on the left side only).

Based on these results, the anatomical features of each blade are summarized below.

○ **Superior frontal blade—**A blade adjacent to the anterior/superior part of the CR and CC. Fibers from the CR, CC, CG, UNC, and IFO merge into this blade. The superior frontal WM, rectus WM, and middle orbito-frontal WM belong to this blade.

○ **Middle frontal blade—**A blade adjacent to the anterior/superior part of the CR. The middle frontal WM belongs to this blade.

○ **Inferior frontal blade—**A blade adjacent to the anterior/superior part of the CR. Fibers from the CR, IFO, and UNC merge into the anterior part this blade, and fibers from the SLF merge into the posterior part of this blade. The inferior frontal WM and the lateral orbito-frontal WM belong to this blade.

○ **Pre-central blade—**A blade adjacent to the superior part of the CR. Fibers from the CST and the SLF merge into this blade. The pre-central WM belongs to this blade.

○ **Post-central blade—**A blade adjacent to the superior part of the CR. Fibers from the CR and the SLF merge into this blade. The post-central WM belongs to this blade.

○ **Superior parietal blade—**A blade adjacent to the posterior part of the CR and the body/splenium of the CC. Fibers from the CR, CC, and CG merge into this blade. The superior parietal WM and precuneus WM belong to this blade.

○ **Parieto-temporal blade—**A blade adjacent to the RLIC and the SS. Fibers from the RLIC and the SLF merge into this blade. The supramarginal WM, angular WM, and superior temporal WM belong to this blade.

○ **Temporal blade—**A blade adjacent to the SS. Fibers from the UNC merge into the anterior part, fibers from the SLF merge into the posterior part, and fibers from the IFO merge into the entire blade. The middle and inferior temporal WMs and the anterior part of the fusiform WM belong to this blade.

○ **Occipital blade—**A blade adjacent to the SS. Fibers from the SS, CC, IFO, and ILF merge into this blade. The superior, middle, and inferior occipital WMs, cuneus WM, lingual WM, and anterior part of the fusiform WM belong to this blade.

Use of the WM atlas as a region-reporting template

The[S13] proposed parcellation map can be used to report locations of specific white matter areas, such as lesion locations. When lesions are located outside of the DWM areas of classical anatomical definition, it has been difficult to define and report the affected white matter areas. Superimposing our parcellation map onto the image of interest would provide a systematic

way for anatomical localization. It is also possible to apply the atlas to quantitative MRI maps such as apparent diffusion constant, FA, eigenvalues, or T2 maps, which are normalized to the ICBM coordinates. Table 3 summarizes results of such operation applied to FA maps of 10 normal subjects not included in the atlas generation. By using our in-house softere (RoiEditor, X. Li, H. Jiang, S. Mori, Johns Hopkins University), FAs of 68 3D white matter regions (50 DWM regions and 18 blades) are automatically measured after affine transformation to the ICBM coordinates. The average and standard deviation values in this table can be used for initial estimation of power analyses.

Discussion

In this study, we investigated SWM structures using DTI. In past investigations, group-averaged DTI has been studied and many common axonal tracts were identified in the DWM regions. The locations and sizes of these structures are reproducible among normal subjects, and they can be clearly identified in the linear-normalized images. The existence of these tracts has been well-documented in numerous anatomical and histological studies (e.g., (Burgel et al., 2006; Dejerine, 1895; Flechsig, 1920)) with their names assigned. In this paper, we extended these efforts to establish atlases of the SWM. This requires identifying common structures in the peripheral regions, where descriptions by previous studies are scarce.

Axons that connect the distal areas of the brain tend to merge with other axons that share similar destinations, forming large bundles in the DWM regions. These prominent WM tracts are major constituents of both the deep and the superficial WM. On the other hand, it has also been documented that there are many cortico-cortical short association fibers that are confined to the SWM regions (Dejerine, 1895; Meynert, 1872). For example, the existence of several short association fibers, such as the vertical occipital fascicle and the orbito-frontal fascicle, has been reported in textbooks, although the exact locations have not been defined (Kahle et al., 1986). The situation is similar for short association fibers that connect adjacent gyri, called the U-fibers of Meynert (Meynert, 1872). The existence of these fibers has also[S14] been demonstrated by neuropathological studies (Cervos-Navarro et al., 1994; Cobb et al., 1950; Kurachi et al., 1999), but locations of U-fibers have not been well identified three-dimensionally in the past. The study of common anatomic structures in the SWM has been further hampered by the significant amount of individual variability in the cortex; deciphering the common and individual-specific structural features would be of great importance and requires group analyses.

Normalization approach for the population-averaged atlas and identified blade structures

For the group analysis of the SWM, we adopted linear brain normalization, which effectively adjusts the overall size of the brain, but leaves details of brain structures not aligned among individuals. With this approach, most large tracts in the DWM can be identified, suggesting that their existence and locations are reproducible (Fig. 1B). On the other hand, this approach cannot align detailed cortical structures adequately, which leads to significant blurring in population-averaged images. For the SWM, which is situated between the DWM and the cortex, we can assume that only prominent common structures are identified with this approach. Therefore, it is possible that there are more SWM structures that are common in normal populations, but unidentified in the present study.

After the normalization, the probabilistic WM map was created by averaging the FA-thresholded images of normal subjects, followed by the identification of the CSWM by probability thresholding. This approach identified blade-like structures of the CSWM, which have simpler structures than the cortices to which they are associated. After averaging linear-normalized images, even the most reproducible gyri, such as pre- and post central gyri, cannot be well-defined. However, the blades underneath these gyri are well defined (Fig. 2).

From the shape of the CSWM, we have identified nine large blades, the structures of which have a close relationship with the cortical structures, as shown in Fig. 4 and Table 1. While[S15] there are some blades that have a one-to-one relationship to cortical areas, several blades include multiple cortical areas per blade (one blade ⊃ one or multiple cortical areas). The only exception is the fusiform WM that spans the temporal blade for the anterior part and the occipital blade for the posterior part. However, based on the definition of the Talairach atlas, the fusiform gyrus is known to consist of at least two regions; one in the temporal lobe and the other in the occipital lobe. Therefore, this result is understandable. We[S16] would like to stress that the nine blades were defined by visual inspection. While some blades have clear structural transitions from one blade to the other, the boundaries of several blades (e.g., the parieto-temporal blade and the occipital blade) have a certain degree of arbitrariness in our definition. This type of arbitrariness is often unavoidable in brain atlases because many anatomical structures inherently do not have clear boundaries.

Identification of SWM tracts that interconnect the blades

Using each blade as an ROI for tractography, we searched for WM tracts that interconnect the blades. Most tracts identified in this approach have already been well-characterized by histology and tractography in the past (Basser et al., 2000; Catani et al., 2002; Conturo et al., 1999; Jellison et al., 2004; Mori et al., 1999; Mori et al., 2002; Mori et al., 2005; Poupon et al., 2000; Stieltjes et al., 2001; Wakana et al., 2004). In addition, we identified four short association fibers and one long association fiber in the population-averaged map and also in individual DTI data. Among these fibers, the fronto-central short association fibers and the central short association fibers are elaborated in the previous studies of human and nonhuman primates (Barbas and Pandya, 1987; Catani et al., 2002; Dejerine, 1895; Leichnetz, 1986; Pandya and Kuypers, 1969; Pandya and Vignolo, 1971). Based on this prior information, they are likely to be real entities. On the other hand, the frontal and the parietal short association fibers and the parieto-temporal long association fibers, which we identified in this study, have not been well-documented previously, even though some of them were depicted rudimentarily in a textbook (Crosby et al., 1962) without specific names. The frontal short association and the parieto-temporal long association fibers were also not clearly recognizable in two to three individuals (out of 10) tested in this study. Therefore, their character remains disputable.

Limitations of diffusion tensor imaging and interpretation of the results

The anatomical information used in this study is based on diffusion tensor imaging, in which measured water diffusion properties are fitted to a simple 3×3 tensor model[S17]. This model, in which it is assumed that there is only one dominant fiber population within each pixel, is an oversimplification (Frank, 2001; Tuch et al., 2002). This could be an issue, especially for the SWM, in which fiber architectures are expected to be more complicated than the DWM. Therefore, we need to be cautious about the interpretation of the tractography results (Fig. 5-7), which is based on fiber orientation information and prone to artifacts. For example, the lack of short association fibers by tractography does not necessarily mean there are no association fibers in such areas. There are two reasons we would expect false negatives. First, with the current image resolution (2.5 mm), we expected a mixture of fibers with multiple populations. In such areas, the FACT algorithm employed in this study provides conservative results (tracking does not penetrate such problematic areas). For[S18] further investigation of the potentially complicated anatomy of the SWM, probabilistic tractography (Behrens et al., 2003; Parker et al., 2002), based on non-tensor models (Frank, 2001; Tuch et al., 2002), would be necessary. Second, the imperfect normalization process also leads to misalignment of small short association fibers. Unless short association fibers are the dominant component in the vicinity, their existence may be covered or averaged out by other more dominant fibers. We also cannot completely exclude a possibility that those short association fibers we identified are false positives. Because the exact coordinates of these short association fibers have not

been well-characterized by previous histology studies, we cannot validate our findings easily. However, there could be several interesting applications based on our results. First, the fact that these fibers can be found by DTI reproducibly means we can identify the corresponding brain locations in the SWM of the normal population. While the blade structures can identify specific WM regions at a more macroscopic level, these short association fibers could define more pin-pointed areas in the SWM. This allows us to study WM (e.g., T2, FA, and ADC) and gray matter (e.g., cortical thickness) features of the areas associated with these short association fibers. Second, if group analyses show that one of the tractography-defined short association fibers are severely altered in a patient group (e.g., cannot be identified or are significantly smaller), such results strongly suggest differences in axonal architectures in the related areas.

Application of this atlas

The identification of common anatomic features of the SWM allows us to investigate the effects of brain diseases on these structures. For[S19] example, we can apply the atlas to report the location of plaques in MS patients. Using a conventional T_1 or T_2-weighted image, the location of the lesion could be reported in absolute coordinates (e.g. x, y, z coordinates in the patient frame) in normalized coordinates, but it is often difficult to relate it to specific white matter anatomy. Our SWM atlas adds new anatomical dimensions to evaluate the frequency of lesions for each white matter areas or to relate lesions locations and functional outcomes. As shown in Table 3, the atlas can be warped into individual subject data for automated brain parcellation, which allows volume and contrast (e.g., FA, ADC, T2, MTR, etc.) measurements in each area.

In this study, we employed affine transformation for brain normalization, which is a valid but crude operation. For example, the standard deviations of FA values reported in Table 3 contain not only the real variability of FA of each structure, but also registration errors. This is apparent for such white matter tracts as the fornix, which are small and registration error would lead to significant measurement inaccuracy. This leads to low statistical power as a quantification tool. If significant differences in FA values are found[S20] between control and patient groups, it could be due to consistent anatomical difference between the two groups and consequent difference in the registration quality. Therefore, the proposed tool should be used as an initial screening and careful inspection and interpretation of the results are required. Employment of a non-linear normalization method is an obvious future direction of this research, which is underway. The atlases developed in this study are now available for downloading from our websites for testing.

In conclusion, we developed a population-based atlas of the SWM using diffusion tensor imaging. The SWM was divided into 9 blade-type structures and their association with cortical areas was described. Based on tractography, several inter-blade tracts were identified. This atlas is expected to be a useful tool to systematically labeling SWM regions.

Acknowledgments

This research was supported by NIH grants P41 RR015241, U24RR021382, PO1 EB00195 and RO1AG20012. The contents are solely the responsibility of the authors and do not necessarily represent the official view of NCRR or NIH. Dr. Peter C.M. van Zijl is a paid lecturer for Philips Medical Systems. This arrangement has been approved by Johns Hopkins University in accordance with its conflict of interest policies.

References

Alexander DC, Pierpaoli C, Basser PJ, Gee JC. Spatial transformations of diffusion tensor magnetic resonance images. IEEE Trans Med Imaging 2001;20:1131–1139. [PubMed: 11700739]

Amunts, K.; Zilles, K., editors. Advances in cytoarchitectonic mapping of the human cerebral cortex. Saunders Company; Philadelphia: 2001.

Axer H, Keyserlingk DG. Mapping of fiber orientation in human internal capsule by means of polarized light and confocal scanning laser microscopy. J Neurosci Methods 2000;94:165–175. [PubMed: 10661836]

Barbas H, Pandya DN. Architecture and frontal cortical connections of the premotor cortex (area 6) in the rhesus monkey. J Comp Neurol 1987;256:211–228. [PubMed: 3558879]

Basser PJ, Mattiello J, LeBihan D. Estimation of the effective self-diffusion tensor from the NMR spin echo. J. Magn. Reson. B 1994;103:247–254. [PubMed: 8019776]

Basser PJ, Pajevic S, Pierpaoli C, Duda J, Aldroubi A. In vitro fiber tractography using DT-MRI data. Magn. Reson. Med 2000;44:625–632. [PubMed: 11025519]

Behrens TE, Johansen-Berg H, Woolrich MW, Smith SM, Wheeler-Kingshott CA, Boulby PA, Barker GJ, Sillery EL, Sheehan K, Ciccarelli O, Thompson AJ, Brady JM, Matthews PM. Non-invasive mapping of connections between human thalamus and cortex using diffusion imaging. Nat Neurosci 2003;6:750–757. [PubMed: 12808459]

Burgel U, Amunts K, Hoemke L, Mohlberg H, Gilsbach JM, Zilles K. White matter fiber tracts of the human brain: three-dimensional mapping at microscopic resolution, topography and intersubject variability. Neuroimage 2006;29:1092–1105. [PubMed: 16236527]

Burgel U, Mecklenburg I, Blohm U, Zilles K. Histological visualization of long fiber tracts in the white matter of adult human brains. J Hirnforsch 1997;38:397–404. [PubMed: 9350511]

Burgel U, Schormann T, Schleicher A, Zilles K. Mapping of histologically identified long fiber tracts in human cerebral hemispheres to the MRI volume of a reference brain: position and spatial variability of the optic radiation. Neuroimage 1999;10:489–499. [PubMed: 10547327]

Catani M, Howard RJ, Pajevic S, Jones DK. Virtual in vivo interactive dissection of white matter fasciculi in the human brain. Neuroimage 2002;17:77–94. [PubMed: 12482069]

Catani M, Jones DK, ffytche DH. Perisylvian language networks of the human brain. Ann Neurol 2005;57:8–16. [PubMed: 15597383]

Cervos-Navarro J, Lafuente JV, Gutierrez E, Kannuki S. Subcortical U-fibers layer preservation in brain edema. Acta Neurochir Suppl (Wien) 1994;60:151–154. [PubMed: 7976531]

Clarke S, Miklossy J. Occipital cortex in man: organization of callosal connections, related myelo- and cytoarchitecture, and putative boundaries of functional visual areas. J Comp Neurol 1990;298:188–214. [PubMed: 2212102]

Cobb S, Pool JL, Scarff J, Schwab RS, Walker AE, White JC. Section of U fibers of motor cortex in cases of paralysis agitans (Parkinson's disease); report of 9 cases. Arch Neurol Psychiatry 1950;64:57–59.

Conturo TE, Lori NF, Cull TS, Akbudak E, Snyder AZ, Shimony JS, McKinstry RC, Burton H, Raichle ME. Tracking neuronal fiber pathways in the living human brain. Proc. Natl. Acad. Sci. USA 1999;96:10422–10427. [PubMed: 10468624]

Crosby, E.; Humphrey, T.; Lauer, E. Correlative anatomy of the nervous system. MacMillan; New York: 1962.

Dejerine, J. Anatomie des centres nerveux. Rueff; Paris: 1895.

Eickhoff S, Stephan KE, Mohlberg H, Grefkes C, Fink GR, Amunts K, Zilles K. A new SPM toolbox for combining probabilistic cytoarchitectonic maps and functional imaging data. Neuroimage 2005;25:1325–1335. [PubMed: 15850749]

Faul F, Erdfelder E, Lang AG, Buchner A. G*Power 3: a flexible statistical power analysis program for the social, behavioral, and biomedical sciences. Behav Res Methods 2007;39:175–191. [PubMed: 17695343]

Flechsig, P. Anatomie des menschlichen Gehirns und Ruchenmarks auf myelogenetischer Grundlage. Thieme; Leipzig: 1920.

Frank LR. Anisotropy in high angular resolution diffusion-weighted MRI. Magn Reson Med 2001;45:935–939. [PubMed: 11378869]

Huang H, Zhang J, van Zijl PC, Mori S. Analysis of noise effects on DTI-based tractography using the brute-force and multi-ROI approach. Magn Reson Med 2004;52:559–565. [PubMed: 15334575]

Jellison BJ, Field AS, Medow J, Lazar M, Salamat MS, Alexander AL. Diffusion tensor imaging of cerebral white matter: a pictorial review of physics, fiber tract anatomy, and tumor imaging patterns. AJNR Am J Neuroradiol 2004;25:356–369. [PubMed: 15037456]

Jiang H, van Zijl PC, J. K, Pearlson GD, Mori S. DtiStudio: resource program for diffusion tensor computation and fiber bundle tracking. Comput Methods Programs Biomed 2006;81:106–116. [PubMed: 16413083]

Jones DK, Horsfield MA, Simmons A. Optimal strategies for measuring diffusion in anisotropic systems by magnetic resonance imaging. Magn. Reson. Med 1999;42:515–525. [PubMed: 10467296]

Kahle, W.; Leonhardt, H.; Platzer, W. Taschenatlas der Anatomie fur Studium and Praxis; Stuttgart: 1986.

Krieg, W. Connections of the cerebral cortex. Brain books; Evanston, IL: 1963.

Kurachi Y, Sakakihara Y, Kubota M, Oka A, Hatakeyama K, Nose K, Yazawa K. Preferential involvement of U-fibers in human herpesvirus 6-associated acute encephalopathy. Ann Neurol 1999;45:684. [PubMed: 10319898]

Leichnetz GR. Afferent and efferent connections of the dorsolateral precentral gyrus (area 4, hand/arm region) in the macaque monkey, with comparisons to area 8. J Comp Neurol 1986;254:460–492. [PubMed: 3805358]

Makris N, Kennedy DN, McInerney S, Sorensen AG, Wang R, Caviness VS Jr. Pandya DN. Segmentation of subcomponents within the superior longitudinal fascicle in humans: a quantitative, in vivo, DT-MRI study. Cereb Cortex 2005;15:854–869. [PubMed: 15590909]

Makris N, Worth AJ, Sorensen AG, Papadimitriou GM, Reese TG, Wedeen VJ, Davis TL, Stakes JW, Caviness VS, Kaplan E, Rosen BR, Pandya DN, Kennedy DN. Morphometry of in vivo human white matter association pathways with diffusion weighted magnetic resonance imaging. Ann. Neurol 1997;42:951–962. [PubMed: 9403488]

Mazziotta JC, Toga AW, Evans A, Fox P, Lancaster J. A probabilistic atlas of the human brain: theory and rationale for its development. The International Consortium for Brain Mapping (ICBM). Neuroimage 1995;2:89–101. [PubMed: 9343592]

Meynert, T., editor. Vom Gehirn der Saugetiere. Engelmann; Leipzig: 1872.

Mori S, Crain BJ, Chacko VP, van Zijl PCM. Three dimensional tracking of axonal projections in the brain by magnetic resonance imaging. Annal. Neurol 1999;45:265–269. [PubMed: 9989633]

Mori S, Kaufmann WE, Davatzikos C, Stieltjes B, Amodei L, Fredericksen K, Pearlson GD, Melhem ER, Solaiyappan M, Raymond GV, Moser HW, van Zijl PCM. Imaging cortical association tracts in human brain. Magn Reson Med 2002;47:215–223. [PubMed: 11810663]

Mori S, Oishi K, Jiang H, Jiang L, Li X, Akhter K, Hua K, Faria AV, Mahmood A, Woods R, Toga AW, Pike GB, Neto PR, Evans A, Zhang J, Huang H, Miller MI, van Zijl P, Mazziotta J. Stereotaxic white matter atlas based on diffusion tensor imaging in an ICBM template. NeuroImage. 2008a

Mori S, Oishi K, Jiang H, Jiang L, Li X, Akhter K, Hua K, Faria AV, Mahmood A, Woods R, Toga AW, Pike GB, Neto PR, Evans A, Zhang J, Huang H, Miller MI, van Zijl P, Mazziotta J. Stereotaxic white matter atlas based on diffusion tensor imaging in an ICBM template. Neuroimage 2008b;40:570–582. [PubMed: 18255316]

Mori, S.; Wakana, S.; Nagae-Poetscher, LM.; van Zijl, PC. MRI atlas of human white matter. Elsevier; Amsterdam, The Netherlands: 2005.

Pandya DN, Kuypers HG. Cortico-cortical connections in the rhesus monkey. Brain Res 1969;13:13–36. [PubMed: 4185124]

Pandya DN, Vignolo LA. Intra- and interhemispheric projections of the precentral, premotor and arcuate areas in the rhesus monkey. Brain Res 1971;26:217–233. [PubMed: 4993847]

Parker GJ, Stephan KE, Barker GJ, Rowe JB, MacManus DG, Wheeler-Kingshott CA, Ciccarelli O, Passingham RE, Spinks RL, Lemon RN, Turner R. Initial demonstration of in vivo tracing of axonal projections in the macaque brain and comparison with the human brain using diffusion tensor imaging and fast marching tractography. Neuroimage 2002;15:797–809. [PubMed: 11906221]

Petrides M, Pandya DN. Projections to the frontal cortex from the posterior parietal region in the rhesus monkey. J Comp Neurol 1984;228:105–116. [PubMed: 6480903]

Pierpaoli C, Basser PJ. Toward a quantitative assessment of diffusion anisotropy. Magn.Reson.Med 1996;36:893–906. [PubMed: 8946355]

Pierpaoli C, Jezzard P, Basser PJ, Barnett A, Di Chiro G. Diffusion tensor MR imaging of human brain. Radiology 1996;201:637–648. [PubMed: 8939209]

Poupon C, Clark CA, Frouin V, Regis J, Bloch L, Le Bihan D, Mangin JF. Regularization of diffusion-based direction maps for the tracking of brain white matter fascicules. Neuroimage 2000;12:184–195. [PubMed: 10913324]

Pruessmann KP, Weiger M, Scheidegger MB, Boesiger P. SENSE: sensitivity encoding for fast MRI. Magn Reson Med 1999;42:952–962. [PubMed: 10542355]

Stieltjes B, Kaufmann WE, van Zijl PCM, Fredericksen K, Pearlson GD, Mori S. Diffusion tensor imaging and axonal tracking in the human brainstem. Neuroimage 2001;14:723–735. [PubMed: 11506544]

Toga AW, Thompson PM, Mori S, Amunts K, Zilles K. Towards multimodal atlases of the human brain. Nat Rev Neurosci 2006;7:952–966. [PubMed: 17115077]

Tuch DS, Reese TG, Wiegell MR, Makris N, Belliveau JW, Wedeen VJ. High angular resolution diffusion imaging reveals intravoxel white matter fiber heterogeneity. Magn Reson Med 2002;48:577–582. [PubMed: 12353272]

Wakana S, Jiang H, Nagae-Poetscher LM, Van Zijl PC, Mori S. Fiber Tract-based Atlas of Human White Matter Anatomy. Radiology 2004;230:77–87. [PubMed: 14645885]

Woods RP, Grafton ST, Holmes CJ, Cherry SR, Mazziotta JC. Automated image registration: I. General methods and intrasubject, intramodality validation. J Comput Assist Tomogr 1998;22:139–152. [PubMed: 9448779]

Xu D, Mori S, Shen D, van Zijl PC, Davatzikos C. Spatial normalization of diffusion tensor fields. Magn Reson Med 2003;50:175–182. [PubMed: 12815692]

Xue R, van Zijl PCM, Crain BJ, Solaiyappan M, Mori S. In vivo three-dimensional reconstruction of rat brain axonal projections by diffusion tensor imaging. Magn. Reson. Med 1999;42:1123–1127. [PubMed: 10571934]

Zilles, K., editor. Architecture of the human cerebral cortex: Regional and laminar organization. Elsevier; Amsterdam: 2004.

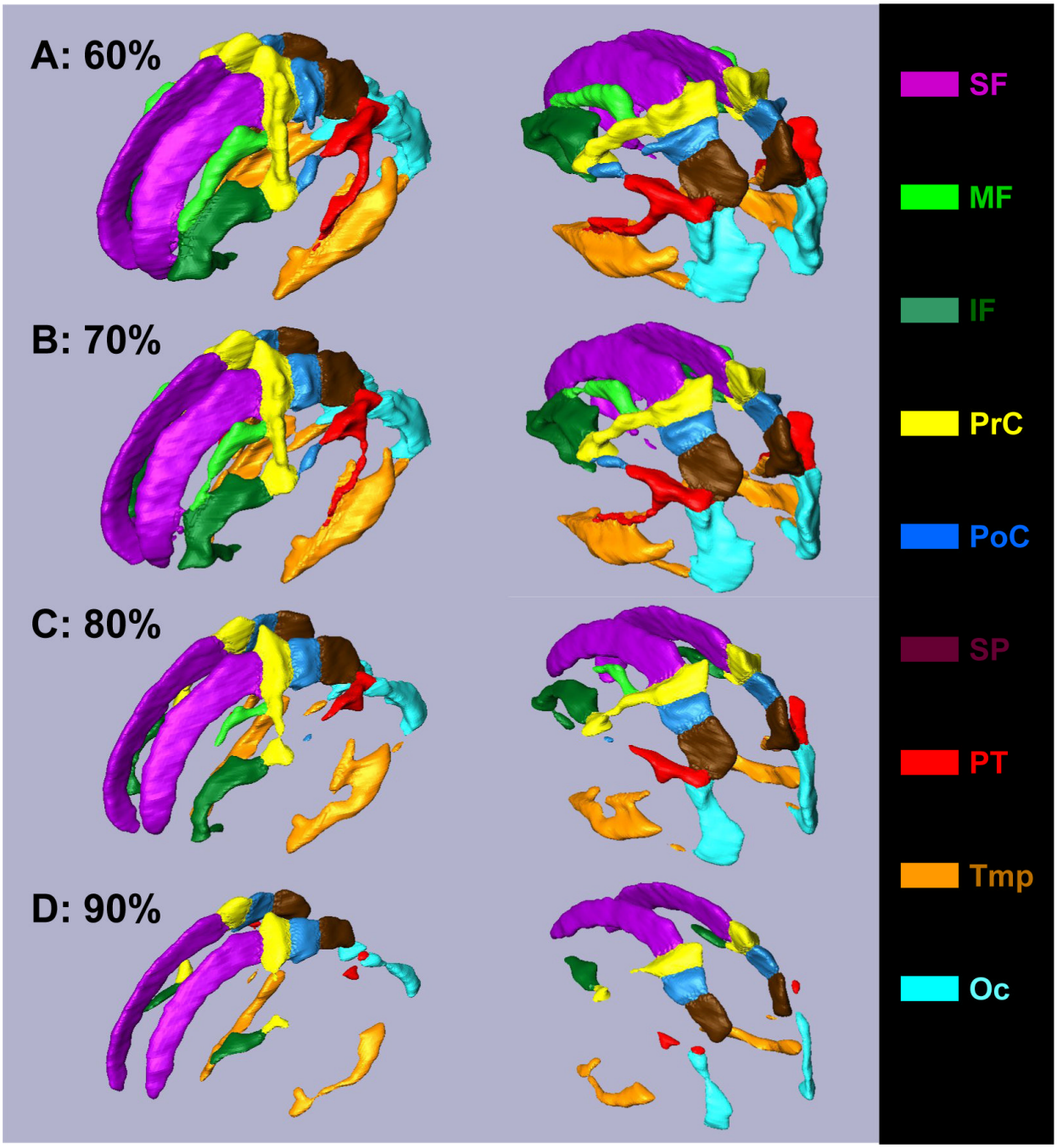

Figure 1.
The ICBM-DTI-81 atlas, hand-segmented DWM structures, and SWM. (A): The ICBM-152 atlas used as a target image to register the DTI data from 81 normal subjects. (B): The ICBMDTI-81 atlas, which was created by linearly averaging the normative DTI data. The hand-segmented WM parcellation map (WMPM) is superimposed. (C): Probabilistic WM map. (D): A 3D view of the WMPM representing the anatomy of the DWM. (E) and (F): 3D views of the SWM, defined by 0.6 white matter probability. Figures[S21] A-D and the WMPM are from our previous publication (Mori et al., 2008b) and are presented in this figure to help visualize the relationship with the SWM.

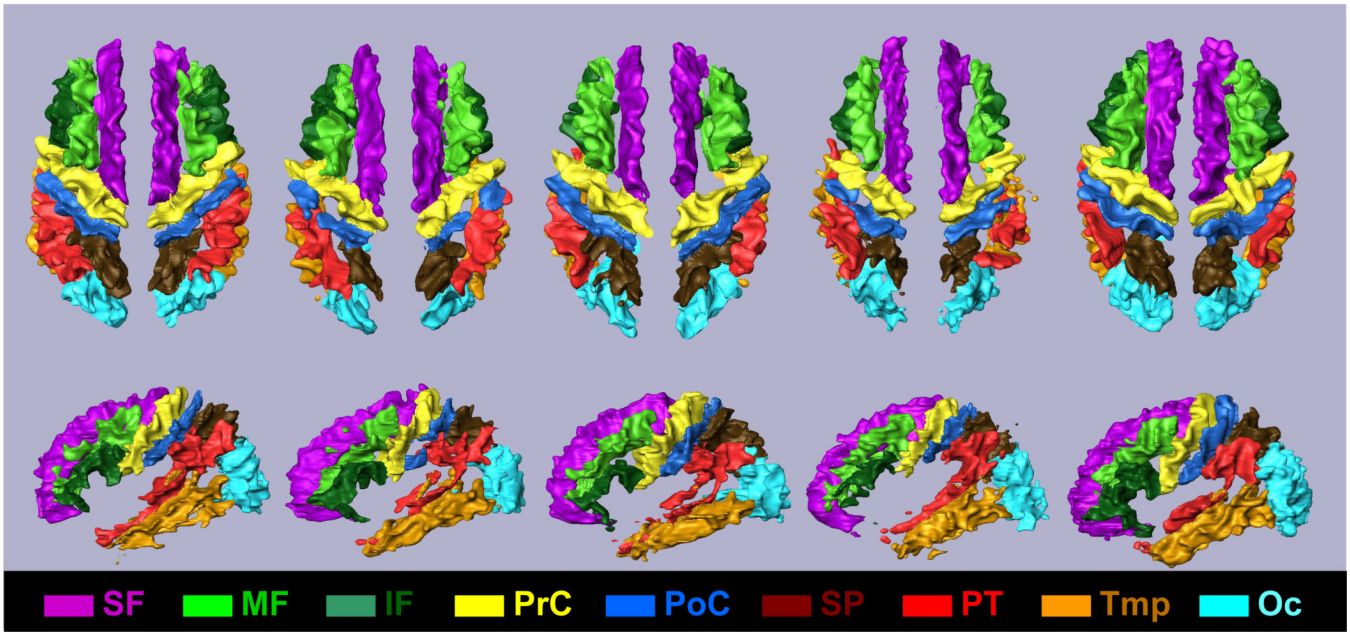

Figure 2.

Nine blade-like structures (blades) defined by different level of the white matter probability in the SWM; A: 60%, B: 70%, C: 80%, and D: 90%. The blades are: superior frontal blade (SF, purple); middle frontal blade (MF, light green); inferior frontal blade (IF, deep green); pre-central blade (PrC, yellow); post-central blade (PoC, blue); superior parietal blade (SP, brown); parieto-temporal blade (PT, red); temporal blade (Tmp, ochre); and occipital blade (OC, light blue).

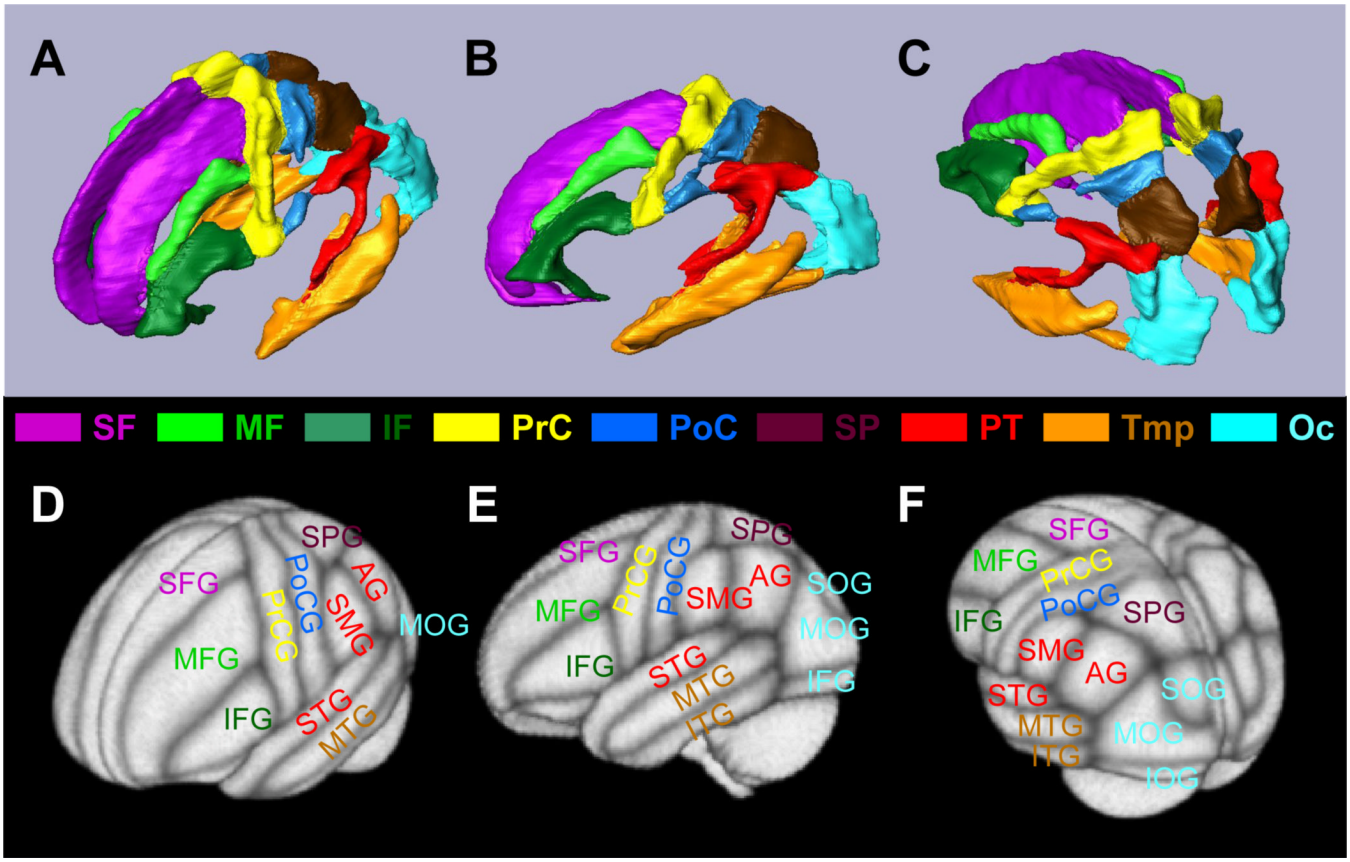

Figure 3.
Results of nine blade identifications in five individual brains. The color assignment is the same as Figure 2.

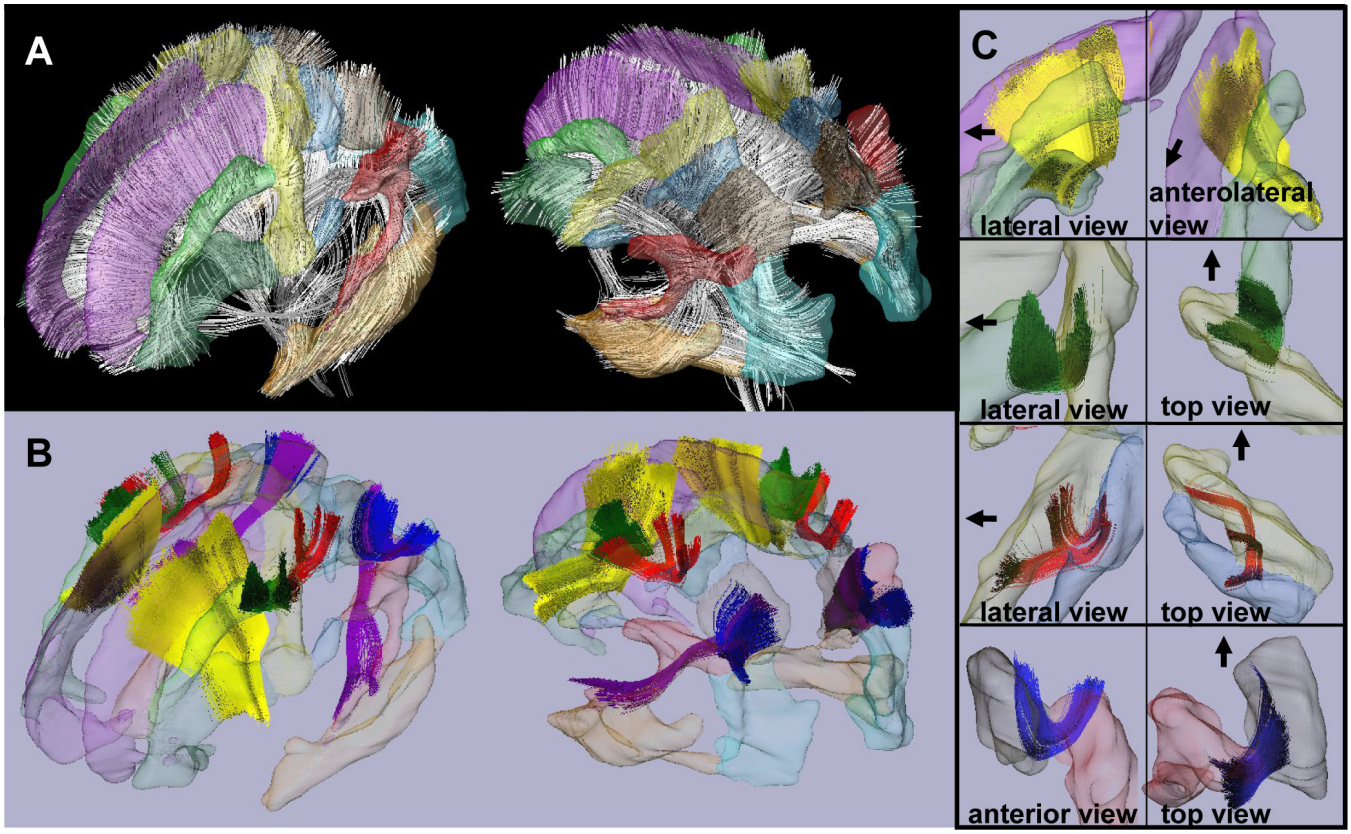

Figure 4.
Comparison of the blade and cortical structures. (A) – (C): Nine blade-like structures (blades) viewed from 3 different angles. (D) – (F): The probabilistic cortical parcellation results obtained from 40 subjects (LPBA40), labeled by the name of gyri. Abbreviations are: SFG, superior frontal girus; MFG, middle frontal girus; IFG, inferior frontal girus; PrCG, pre-central girus; PoCG, post-central girus; SPG; superior parietal girus; SMG, supramarginal girus; AG, angular girus; STG; superior temporal girus; MTG, middle temporal girus; ITG, inferior temporal girus; SOG, superior occipital girus; MOG, middle occipital girus; IFG, inferior occipital girus. The names of the gyri are color-coded based on the color assignment of the blades.

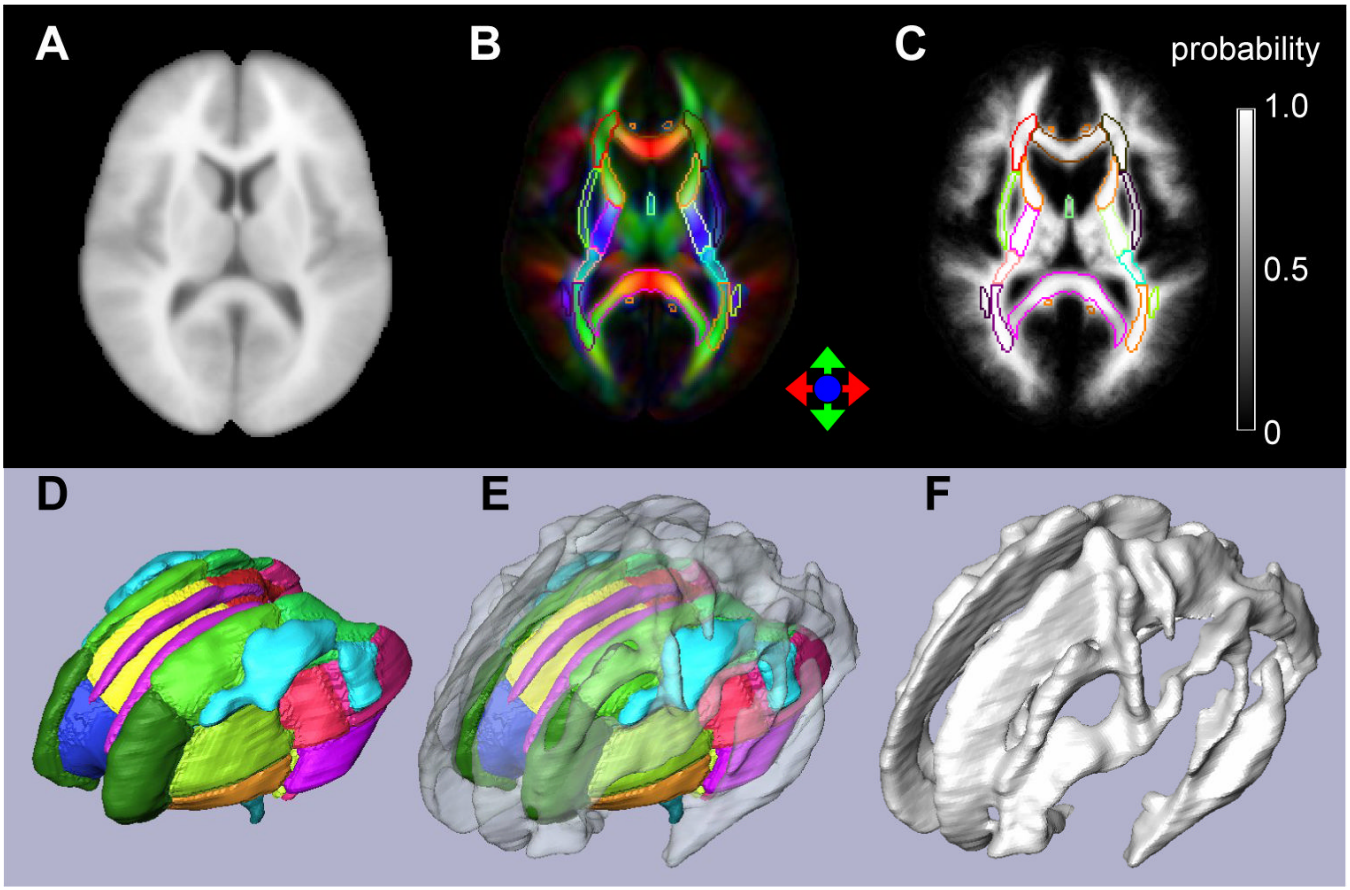

Figure 5.

Inter-blade connectivity studies with tractography. (A): Overall fiber structures in the SWM. In most of the blade-like structures, the fiber orientation is aligned along the radial orientation and intra-blade fibers could not be located. (B): Results of inter-blade tract reconstruction. The four short association fibers identified in this study are: frontal short association fiber (yellow); fronto-central short association fibers (green); central short association fibers (red); and parietal short association fibers (blue) . The one long association fiber, the parieto-temporal long association fiber, is shown in purple. (C): Detailed views of the four short association fibers in the left side; the arrow indicates the orientation of the front of the brain.

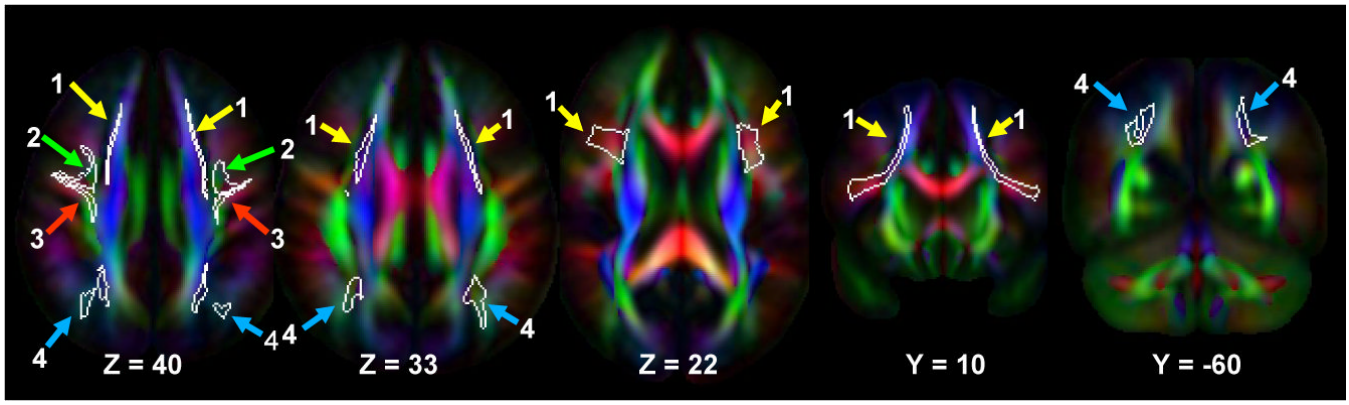

Figure 6.
Locations of the four short association fibers in the ICBM-DTI-81 atlas (ICBM-152 coordinates). The yellow (1), green (2), red (3), and blue (4) arrows indicate the locations of the frontal, fronto-central, central, and parietal association fibers, respectively. The Y and Z slice locations are defined by the distance (mm) from the anterior commissure.

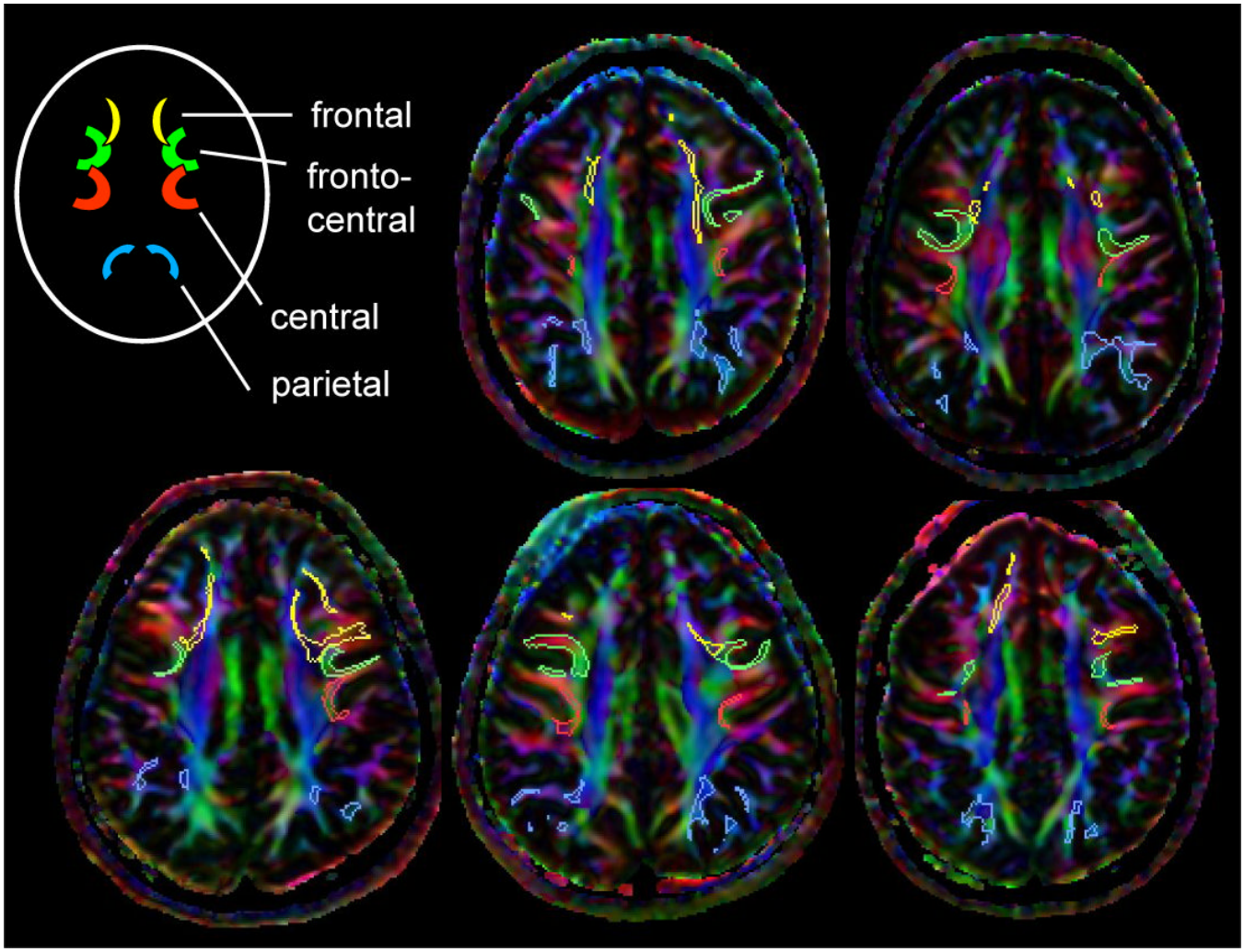

Figure 7.
Identification of the four short association fibers in individual brains. Results from five normal individuals, not included in the ICBM-DTI-81, are shown. The color assignment is the same as Fig. 5.

Table 1

Relationship between the blades , lobes, and subparcellation (Fig. 4)

Blades	Lobes	Subparcellation
Superior frontal blade	Frontal lobe	Superior frontal WM, rectus WM, middle orbito-frontal WM
Middle frontal blade	Frontal lobe	Middle frontal WM
Inferior frontal blade	Frontal lobe	Inferior frontal WM, lateral orbito-frontal WM
Pre-central blade	Frontal lobe	Pre-central WM
Post-central blade	Parietal lobe	Post-central WM
Superior parietal blade	Parietal lobe	Superior parietal WM, precuneus WM
Parieto-temporal blade	Parietal and temporal lobe	Supramarginal WM, angular WM, superior temporal WM
Temporal blade	Temporal lobe	Middle temporal WM, inferior temporal WM, anterior part of fusiform WM
Occipital blade	Occipital lobe	Superior occipital WM, middle occipital WM, inferior occipital WM, cuneus WM, lingual WM, posterior part of fusiform WM

Table 2

Long (upper case) and short (lower case) cortico-cortical association fibers connecting each blade as defined by tractography

	Superior frontal	**Middle frontal**	**Inferior frontal**	**Pre-central**	**Post-central**	**Superior parietal**	**Parieto-temporal**	**Temporal**	**Occipital**
Superior frontal		n/a	fsaf	CG	CG	CG, IFO	UNC	UNC	IFO
Middle frontal			n/a	fcsaf	n/a	IFO	n/a	n/a	IFO
Inferior frontal				n/a	n/a	IFO	SLF-II/Ar	UNC, SLF-Ar	IFO
Pre-central					csaf	CG, SLF-I	SLF-II/Ar,	SLF-Ar	n/a
Post-central						CG, SLF-I	SLF-II/Ar	SLF- Ar	n/a
Superior parietal							psaf, PTLAF	PTLAF	n/a
Parieto-temporal								SLF-Ar	ILF
Temporal									ILF
Occipital									

Note: fsaf: frontal short association fibers; fcsaf: fronto-central short association fibers; csaf: central short association fibers; psaf: parietal short association fibers; PTLAF: parieto-temporal long association fibers; Ar: arcuate fiber: CG: cingulum; IFO: inferior fronto-orbital fascicle; ILF: inferior longitudinal fascicle; SLF: superior longitudinal fascicle; n/a: not applicable

Table 3

Average FAs and standard deviations of 68 white matter areas obtained from 10 normal subjects.

areas	ave	SD	N*	areas	ave	SD	N*	area	ave	SD	N*
MCP	0.36	.06	14	ACR-L	0.39	.06	15	UNC-R	0.38	.11	38
PCT	0.40	.04	6	SCR-R	0.41	.03	4	UNC-L	0.38	.09	28
GCC	0.53	.09	15	SCR-L	0.40	.03	5	TAP-R	0.45	.09	20
BCC	0.46	.12	41	PCR-R	0.39	.02	3	TAP-L	0.44	.10	30
SCC	0.53	.07	11	PCR-L	0.39	.03	6	SF_R	0.35	.03	6
FX	0.42	.11	33	PTR-R	0.44	.03	4	SF_L	0.38	.05	8
CST-R	0.46	.04	6	PTR-L	0.44	.03	4	MF_R	0.31	.05	14
CST-L	0.44	.05	7	SS-R	0.44	.07	14	MF_L	0.32	.04	9
ML-R	0.51	.03	7	SS-L	0.43	.05	9	IF_R	0.32	.06	19
ML-L	0.49	.04	6	EC-R	0.36	.04	8	IF_L	0.34	.07	24
ICP-R	0.36	.05	12	EC-L	0.35	.06	18	PrC_R	0.32	.05	13
ICP-L	0.35	.04	7	CGC-R	0.38	.05	11	PrC_L	0.35	.04	8
SCP-R	0.43	.09	26	CGC-L	0.38	.05	12	PoC_R	0.33	.03	5
SCP-L	0.43	.10	33	CGH-R	0.26	.08	49	PoC_L	0.35	.04	7
CP-R	0.53	.06	9	CGH-L	0.28	.08	48	SP_R	0.33	.05	12
CP-L	0.53	.06	9	FX/ST-R	0.42	.07	16	SP_L	0.35	.03	5
ALIC-R	0.46	.03	4	FX/ST-L	0.40	.06	12	PT_R	0.26	.04	14
ALIC-L	0.43	.07	18	SLF-R	0.37	.05	9	PT_L	0.28	.03	7
PLIC-R	0.55	.03	3	SLF-L	0.36	.05	12	Tmp_R	0.33	.02	4
PLIC-L	0.52	.04	5	SFO-R	0.39	.07	17	Tmp_L	0.33	.03	6
RLIC-R	0.46	.05	7	SFO-L	0.41	.05	8	Oc_R	0.31	.02	4
RLIC-L	0.45	.04	6	IFO-R	0.36	.06	17	Oc_L	0.32	.03	6
ACR-R	0.38	.03	5	IFO-L	0.36	.06	14				

ave: average FA, L: left, R: right, SD: standard deviation. Abbreviations for the area are described in result section.

**: The CSWM is defined by 60% white matter probability.

* The number of subjects required to detect 20% change with $p < 0.05$ using t-test. The software G*power (Faul et al., 2007) was used to determine required sample size, assuming that the size and SD of the control group and subject group are same.